Detector R& D for future Neutrino Experiments with the NUMI Beamline

by Future Neutrino Experiments Study Groupies
Asterisks means those persons have agreed to serve...

Contents

I. INTRODUCTION

Although we as a field have been trying to detect neutrinos for a very long time, the diferent techniques we use are highly constrained by the fact that neutrinos are so very weakly interacting. As an example, consider the historic first and the most recent reactor neutrino detector: Reines and Cowan used 17 tons of liquid scintillator instrumented with phototubes to see the neutrinos from the XXX reactor, and KAMLAND is using 1000 tons of liqiud scintillator instrumented with phototubes to see neutrinos from reactors located all over Japan. Of course the light collectors have improved and expanded, the timing, electronics, and data acquisition has improved, but the fundamental technique for studying reactor neutrinos has not changed.

Just as the topology of neutrino interactions changes dramatically as the neutrino energy increases, so too does the detector technology. At the high energy limit (above a few GeV), neutrinos simply break apart the nucleus and one can measure the incoming neutrino energy from a charged current interaction by calorimetric sampling measurements of the final state particles, which are classified as either the outgoing lepton, or the "hadronic shower". Again, the MINOS detector today is not fundamentally different from the E1A experiment at Fermilab, which measured neutrino interactions calorimetrically with mineral oil-based scintillator and spark chambers, followed by an iron spectrometer. MINOS combines the spectrometer and calorimeter functions, but the detector concept has not changed.

What we have learned in the past many years of neutrino experimentation is that different detectors are suitable for different energy regimes. In this document we will discuss detectors which are being considered for use in the 1-3 GeV regime, in other words, the regime between the two extremes described above. This regime is suitable for experiments which are off the axis of the NUMI beamline, which are very well-positioned to take the next steps in neutrino oscillation physics.

II. NUMI OFF AXIS NEUTRINO SPECTRA

The NUMI beamline is designed to produce relatively wide-band neutrino beams of peak energy ranging anywhere between 3.5 and 14GeV. Its focusing system consist of two horns, which, depending on their relative spacing and their spacing from the NUMI target, can focus pions of varying momentum ranges. Because muon neutrinos come predominantly from 2-body pion (and a few kaon) decays, the neutrino energy at a far detector is determined simply by geometry and kinematics:

$$E_\nu = \gamma m_h * \frac{m_h^2 - m_\mu^2}{m_h^2} * \frac{1}{1 + \theta^2\gamma^2}$$

where γ is simply the parent meson's relativistic boost

III. THEORETICAL MOTIVATIONS

In a modern theoretical context, one generally expects nonzero neutrino masses and associated lepton mixing. There is currently strong experimental evidence for neutrino masses and mixing. One source of this evidence is from solar neutrino experiments, most recently, SuperKamiokande and SNO [1]. This data can be fit by oscillations of the solar ν_e's into ν_μ and ν_τ, with the relevant $\Delta m^2_{21} = m(\nu_2)^2 - m(\nu_1)^2 \simeq 5 \times 10^{-5}$ eV^2 and mixing angle $\tan^2\theta_{12} \simeq 0.4$ [2]. Strong evidence also comes from atmospheric neutrino experiments, especially SuperKamiokande [3], with confirming results from Soudan-2 and MACRO. The atmospheric neutrino data can be fit by $\nu_\mu \to \nu_\tau$ oscillations with $|\Delta m^2_{32}| \simeq 2.5 \times 10^{-3}$ eV^2 and maximal mixing, $\sin^2 2\theta_{23} = 1$ [3]. A pioneering long-baseline accelerator neutrino oscillation experiment, K2K [4], has obtained data consistent with SuperKamiokande results. The sum of data from these experiments can be explained in terms of oscillations involving the three neutrinos ν_e, ν_μ, and ν_τ, members of electroweak doublets. This data excludes light electroweak-singlet ("sterile") neutrinos as playing a large role in the oscillations. There is also a reported observation of $\bar{\nu}_\mu \to \bar{\nu}_e$ oscillations by the LSND experiment [6], which is not confirmed, but also not completely excluded, by the similar KARMEN experiment [7]. The LSND claim will be tested by the MiniBooNE experiment at Fermilab [8], which is currently in an early commissioning phase, and expects to present definitive results in about two years.

In the standard model generalized to include neutrino masses and without mixing with light sterile neutrinos, the weak leptonic charged current has the form $J_\lambda = \bar{\nu}_L U \gamma_\lambda \ell_L$, where the vector of neutrino mass eigenstates is $\nu = (\nu_1, \nu_2, \nu_3)$ and the analogous vector of charged lepton mass eigenstates is $\ell = (e, \mu, \tau)$. The 3×3 unitary lepton mixing matrix U depends on three Euler rotation angles θ_{12}, θ_{13}, and θ_{23}, and a phase δ, all of which can be probed in neutrino oscillation experiments, and (potentially) two other Majorana phases which cannot be directly tested. For $|\Delta m^2_{23}| \gg \Delta m^2_{12}$ and ignoring matter effects, the probability for $\nu_\mu \to \nu_\tau$ is

$$P(\nu_\mu \to \nu_\tau) = \sin^2(2\theta_{23}) \cos^4\theta_{13} \sin^2\phi_{32} \tag{3.1}$$

where

$$\phi_{ij} = \frac{\Delta m^2_{ij} L}{4E} \tag{3.2}$$

and $\Delta m^2_{ij} = m(\nu_i)^2 - m(\nu_j)^2$. Since the best fit to the SuperKamikande data has maximal mixing, it follows that $\theta_{23} \simeq \pi/4$ and $\theta_{13} \ll 1$. The latter constraint also arises from the CHOOZ reactor antineutrino experiment [5]. The CHOOZ limit is dependent on the input value used for $|\Delta m^2_{32}|$; for the current central value 2.5×10^{-3} eV^2, this is $\sin^2(2\theta_{13}) < 0.11$, while for $|\Delta m^2_{32}| = 2.0 \times 10^{-3}$ eV^2, it is $\sin^2(2\theta_{13}) < 0.18$ [5].

The evidence for neutrino oscillations, and hence neutrino masses and lepton mixing, constitutes the first confirmed indication for physics beyond the standard model since its establishment more than 25 years ago. This has led to an intensive program of experimentation to explore further this physics. Fermilab is strongly positioned in this program with the MiniBooNE experiment now beginning data-taking [8] and the MINOS experiment under construction [9]. MINOS will use a neutrino beam with an energy of order a few GeV, traversing a pathlength of $L = 732$ km, from Fermilab to Soudan, MN and will perform several very important measurements, including (i) ν_μ charged-current event rate and energy spectrum, which will check the results of the atmospheric neutrino experiments and is expected to measure the values of $\sin^2 2\theta_{23}$ and $|\Delta m^2_{32}|$ to about 10 %, and (ii) the ν_μ neutral-current event rate, which will provide a cross-check on the oscillation fit and put constraints on the involvement of light electroweak-singlet neutrinos in the oscillations. The proton beam intensity is anticipated to be between about 0.25 MW and 0.4 MW. The above sensitivities are based on 10 kton-yrs of data, i.e. about 2 yrs with the 5 kton MINOS detector. The MINOS program is nicely complementary to the CERN-Gran Sasso neutrino program, in which the OPERA experiment is designed to explicitly detect τ appearance [10]. In Japan, the rebuilding of SuperKamiokande is underway, and the K2K experiment is expected to begin running again in late 2002. Beyond this, there is an ambitious long-baseline neutrino oscillation experiment that plans to use an intense ν_μ beam from the Japan Hadron Facility JHF which will traverse a distance of 295 km to the fully rebuilt SuperKamiokande detector

[11] (JHF-SK). This beam will have an energy $\lesssim 1$ GeV and be produced by an intense 0.77 MW proton beam at JHF. The JHF-SK experimental program envisions measurements of ν_μ disappearance to get high-precision determinations of $|\Delta m^2_{32}|$ and $\sin^2 2\theta_{23}$ and a search for $\nu_\mu \to \nu_e$ oscillations down to a sensitivity of $\sin^2\theta_{13}$ of 0.0015 [11] (see further below). Assuming requisite funding for beamlines, etc. the JHF-SK experiment expects to start commissioning in 2007-2008. Later running with a $\bar{\nu}_\mu$ beam is also planned, and consideration has been given to a second phase of the JHF-Kamioka neutrino program involving the construction of a very large 1 Mton water Cherenkov detector, HyperKamiokande.

Given the large investment that the U.S. high-energy physics community has made in MINOS, and the fact that, together with MiniBooNE, it will be the center of the domestic U. S. accelerator neutrino program during the next 10 years, there is strong motivation for planning upgrades and extensions of this experiment. Several studies have discussed the physics that could be accessed with a higher-intensity conventional neutrino beam, also involving upgrades to the proton intensity, at Fermilab [12]- [19]. Earlier related efforts studied the physics reach of a neutrino factory, including the U.S. studies [20,21] and related studies in Europe and Japan. In the U. S. an effort is also underway to study the physics potential of long-baseline neutrino oscillation experiments using the BNL AGS, upgraded from 0.14 MW to 0.5 MW, with a very large, multi-hundred kton water Cherenkov far detector [21,22].

Here we address research and development for a second far detector using the MINOS beam and optimized for the study of $\nu_\mu \to \nu_e$ oscillations. In vacuum (e.g. [13,14])

$$\begin{aligned}
P(\nu_\mu \to \nu_e) &= 2\sin(2\theta_{13}) s_{23} c_{13} s_{12} (s_{12} s_{23} s_{13} - c_{12} c_{23} c_\delta) \sin^2\phi_{32} \\
&+ 2\sin(2\theta_{13}) s_{23} c_{13} c_{12} (c_{12} s_{23} s_{13} + s_{12} c_{23} c_\delta) \sin^2\phi_{31} \\
&- 2\sin(2\theta_{12}) c_{13}^2 \Big[s_{12} c_{12} (s_{13}^2 s_{23}^2 - c_{23}^2) + s_{13} s_{23} c_{23} (s_{12}^2 - c_{12}^2) c_\delta \Big] \sin^2\phi_{21} \\
&+ \frac{1}{2}\sin(2\theta_{12})\sin(2\theta_{13})\sin(2\theta_{23}) c_{13} s_\delta \Big[\sin\phi_{32}\cos\phi_{32} \\
&- \sin\phi_{31}\cos\phi_{31} + \sin\phi_{21}\cos\phi_{21} \Big],
\end{aligned} \tag{3.3}$$

while the same expression applies for $P(\bar{\nu}_\mu \to \bar{\nu}_e)$ after performing $\delta \to -\delta$.

In the limit $\Delta m^2_{12} \to 0$ (this applies if the solution to the solar neutrino puzzle is in the LOW region),

$$P(\nu_\mu \to \nu_e) = \sin^2(2\theta_{13}) \sin^2\theta_{23} \sin^2\phi_{32}, \tag{3.4}$$

in vacuum. Hence, since one knows $\sin^2\theta_{23}$ and $|\Delta m^2_{32}|$ moderately well from the atmospheric neutrino data (and these determinations will become more accurate with MINOS), it follows that a measurement of, or search for, $\nu_\mu \to \nu_e$ will immediately yield the value of, or a limit on, $\sin^2(2\theta_{13})$.

In general, however, (this applies if the solution to the solar neutrino puzzle is in the LMA region, which is favored by the current solar neutrino data) several of the terms in Eq. (3.3) can be of the same order of magnitude. In this case, a signal for $\nu_\mu \to \nu_e$ (or lack thereof) does not easily translate into a clean measurement of (or upper bound on) θ_{13}, unless all other parameters are precisely known. It should also be noted that, if matter effects [23] are important, the survival probabilities will also depend on another observable, namely the neutrino mass hierarchy, which we choose to parametrize by the sign of Δm^2_{23}. (Whether matter effects are visible depends on the energy of the neutrino beam and on the baseline length; they tend to be more important for higher energies and longer pathlengths.) This ultimately implies that, in order to determine or constrain θ_{13}, it is necessary also to determine several other neutrino oscillation parameters, including the neutrino mass hierarchy and the CP-odd phase δ. This can only be achieved by comparing different channels (neutrino and antineutrino oscillations) and/or different neutrino beams and different baselines.

Turning the picture around, the study of the subleading $\nu_\mu \to \nu_e$ transition untimately enables (indeed, requires) one to explore leptonic CP violation. This leptonic CP violation involves the phase δ (and two Majorana phases which cannot be directly probed with neutrino oscillations) and is measured by the rephasing-invariant quantity [26] determined via the product $Im(U_{ij}U_{kn}U^*_{in}U^*_{kj})$,

$$J = \frac{1}{8}\sin(2\theta_{12})\sin(2\theta_{23})\sin(2\theta_{13})\cos\theta_{13}\sin\delta \tag{3.5}$$

Because one knows that $\sin^2 2\theta_{23} \simeq 1$ from the atmospheric data and $\sin^2 2\theta_{12} \simeq 0.8$ in the LMA fit to the solar data, it follows that J in the leptonic sector may be much larger than its value of few $\times 10^{-5}$ in the quark sector. Furthermore, the values of $|\Delta m^2_{32}|$ and Δm^2_{21} are such that the corresponding three neutrino mass eigenstates are sufficiently large and nondegenerate so as to allow possible experimental exploration of leptonic CP violation in long-baseline neutrino oscillation experiments. It should be noted that comparison of neutrino and antineutrino oscillations also allows one to probe violation of CPT [27].

The MINOS far detector is comprised of magnetized iron slabs with plastic scintillator and is a course-grained sampling calorimeter with muon ID and momentum measurement. It can provide some modest sensitivity to $\nu_\mu \to \nu_e$ oscillations but is not optimized for this. A major background is neutral current π^0 production, since it is difficult to distinguish the shower produced by the π^0 from the shower produced by an electron. The search for $\nu_\mu \to \nu_e$ oscillations motivates planning and constructing a second, fine-grained, far detector which would take advantage of the NuMI beam. To reduce the high-energy part of the neutrino flux and thereby reduce backgrounds to this search due to neutral current π^0 production, the use an off-axis position for this second far detector becomes ideal.

The physics goals of this program would thus include the following:

- Further measurement of ν_μ disappearance and determination of $|\Delta m^2_{32}|$ and $\sin^2 2\theta_{23}$ to higher accuracy.

- Search for $\nu_\mu \to \nu_e$. In order for this Fermilab-based program to be worthwhile, it should be designed to be as sensitive as the projections stated for the JHF-SK program, which are to be sensitive to values of $\sin^2\theta_{13}$ down to 0.0015 [11].

- Given that some interesting baselines are quite long, of order 10^3 km (assuming that the typical neutrino energies explored will be above 1 GeV), the study of matter effects (which is possible if one runs both neutrino and antineutrino beams) should allow the determination of the neutrino mass hierarchy. Such a measurement cannot be performed by the JHF-SK experiment in Japan, as currently envisioned [11]. It should be noted that this is obtainable even of the solution to the solar neutrino puzzle is not in the LMA region [18].

- With sufficiently accurate knowledge of Δm^2_{32}, $\sin^2 2\theta_{23}$, Δm^2_{21}, and $\sin^2 2\theta_{12}$, it may be possible to obtain significant information on the CP-violating phase δ. This will require analysis of certain parameter ambiguities [28] and of matter effects [23]- [25], and the sensitivity will depend on the pathlength(s) of the experiment.

Given this possible physics potential, there is more than enough motivation to carry out an R&D study of various promising types of detectors and simulations of their response. A study group has been meeting at Fermilab for the past year to discuss this. Recently one report was submitted [29]. We believe that it is clear that this work should be pursued with further R&D.

IV. DETECTOR ISSUES AND COMPARISON

A. Detector Requirements for θ_{13}

1. Neutral Current Rejection in a superbeam

2. Intrinsic ν_e Rejection in a superbeam

It's the Energy resolution!

3. Charge identification in a neutrino factory

B. Operation at the Surface

C. Expandability

D. Cost comparisons

E. Fiducial vs Total Mass

V. TOTAL ABSORPTION DETECTORS

A. Liquid Argon Detectors

B. Liquid Argon TPC

Among the options for a large neutrino detector, a liquid argon time projection chamber (TPC) [32] provides the greatest amount of information, in the form of fine-grain tracking as well as total-absorption calorimetry, via a very simple mechanical structure which is therefore very cost-effective when implemented on a large scale.

The power of a liquid argon detector is especially noteworthy for detection of charged-current electron-neutrino interactions of 0-2 GeV, where detailed tracking provides excellent rejection against neutral-current muon-neutrino interactions with a final-state π^0. Hence, it is the most effective detector per unit mass for $\nu_\mu \to \nu_e$ appearance measurements (of $\sin^2 2\theta_1 3$, the sign of Δm^2_{23}, CP violation, ...) in a low-energy neutrino beam such as NUMI, as illustrated in Fig. 1.

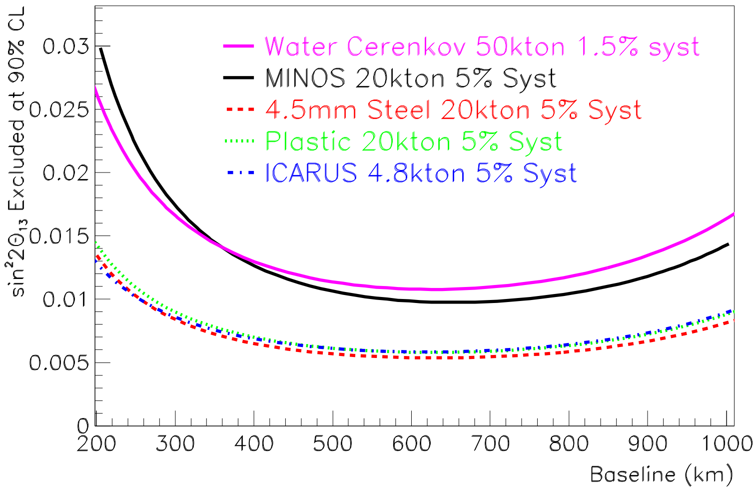

FIG. 1. Comparison of several types of detectors in measuring $\sin^2 2\theta_{13}$ in the presence of backgrounds typical of a pion-decay neutrino beam of 1.5-2 GeV at intermediate baselines [33]. The detector labeled ICARUS [34] is a liquid argon time projection chamber. With a 25-kton liquid argon detector, and an off-axis NUMI neutrino beam, the sensitivity to $\sin^2 2\theta_{13}$ would be 0.002.

FIG. 2. The concept of a liquid argon time projection chamber, as implemented by the ICARUS Collaboration [34]. From [35].

A liquid argon detector is a total absorption calorimeter with time-projection readout via the signal of drifting electrons collected in crossed planes of wires, as sketched in Fig. 2 The effective pixel size is about $5 \times 5 \times 1$ mm^3, compared to the radiation length of 14 cm and nuclear interaction length of 55 cm. At a drift field strength of 500 V/cm, the drift velocity is about 1 mm/μs, so the drift time over, say, 5 m would be 5 ms. Even if operated at the Earth's surface with no shielding, a liquid argon TPC has only about 1 (localized) cosmic-ray track per m^2 of horizontal surface per drift time, so events appear very clean, as shown in Fig. 3.

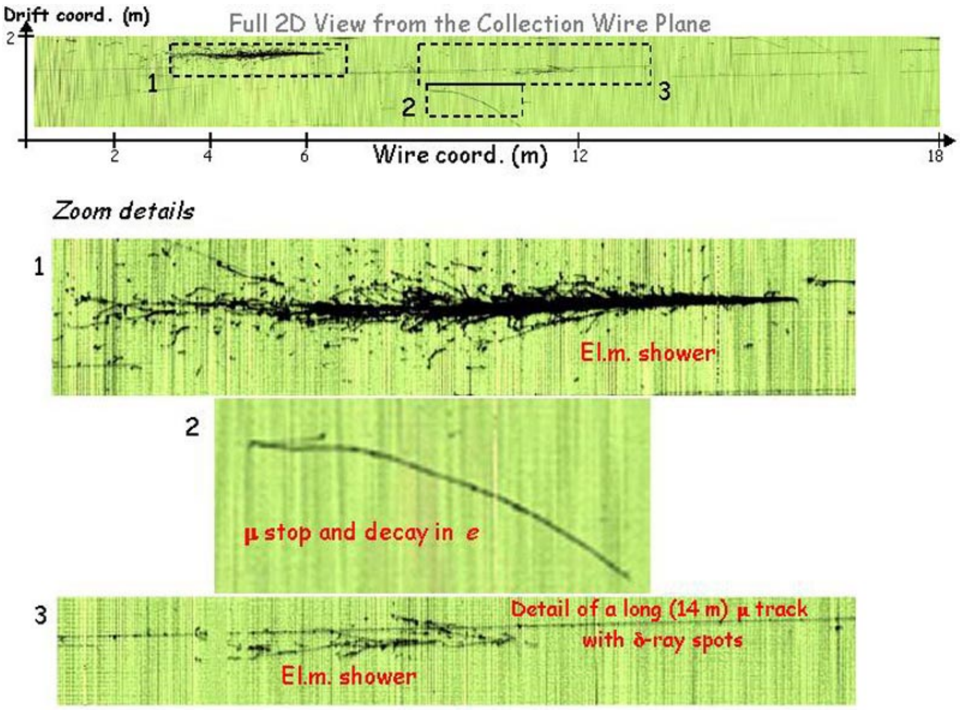

FIG. 3. An event from the recent cosmic-ray test run of ICARUS [34], showing excellent track resolution over long drift distances in zero magnetic field (and low "accidental" cosmic-ray backgrounds in a detector on the Earth's surface).

A liquid argon detector of 100 ktons or more also has competitive capability for nucleon decay searches [38], particularly because it has high efficiency for the decay $p \to K^+\bar{\nu}_\mu$ that is favored in many SO(10) SUSY models [39], as well as for atmospheric, solar and supernova neutrino physics. However, pursuit of these additional physics topics will likely require the detector to be sited underground, at considerable additional expense. Here, we emphasize a detector on the surface for use in a pulsed neutrino beam.

The reliability and stability of their electronic readout has led to the use of liquid argon calorimeters in numerous electron and hadron beam experiments over the past 20 years. A liquid argon TPC differs from these sampling calorimeters in having a long (2-5 m $\Leftrightarrow$ 2-5 msec) drift length. For stable operation over a long drift path the oxygen content of the liquid argon must be less than 0.1 ppb [40], which can be maintained by continuous filtration of the argon (both in liquid phase and in the boiloff/recondensation phase) using commercial Oxisorb cartridges [41].

To obtain economies of scale, a large liquid argon detector should be implemented in a single cryostat, such as those commonly used in the liquefied natural gas industry. Cryogenic volumes of up to 200,000 m^3 (= 280 kton if liquid argon) are now in use, as sketched in Fig. 4.

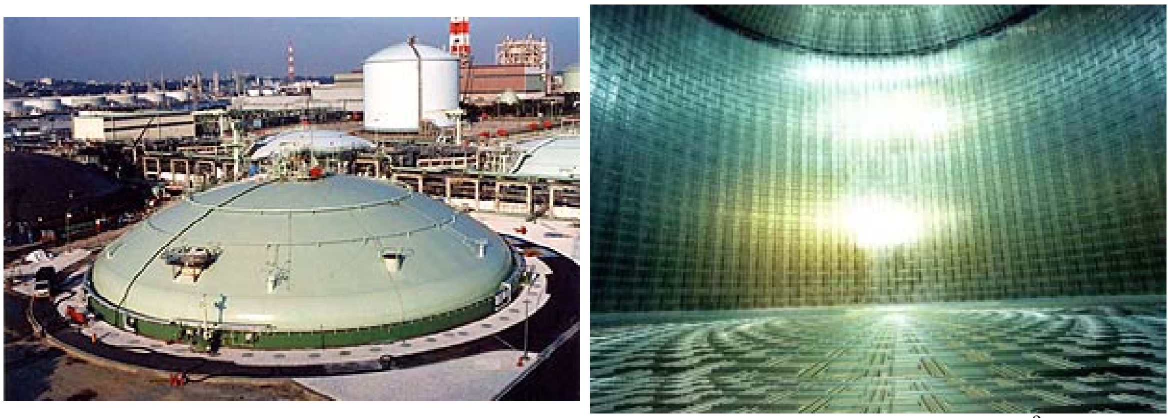

FIG. 4. Photographs of cryogenic storage tanks of volumes $\approx 200,000$ m^3.

An overall concept of a large liquid argon detector is shown in Fig. 5. The diameter of a large liquid argon detector will be greater than (twice) the maximum drift distance (≈ 5 m as limited by oxygen impurities), so the readout must consist of a set of parallel anode and cathode planes that subdivide the detector, as shown in Figs. 5 and 6. Then, the number of readout channels scales as the surface area of the detector.

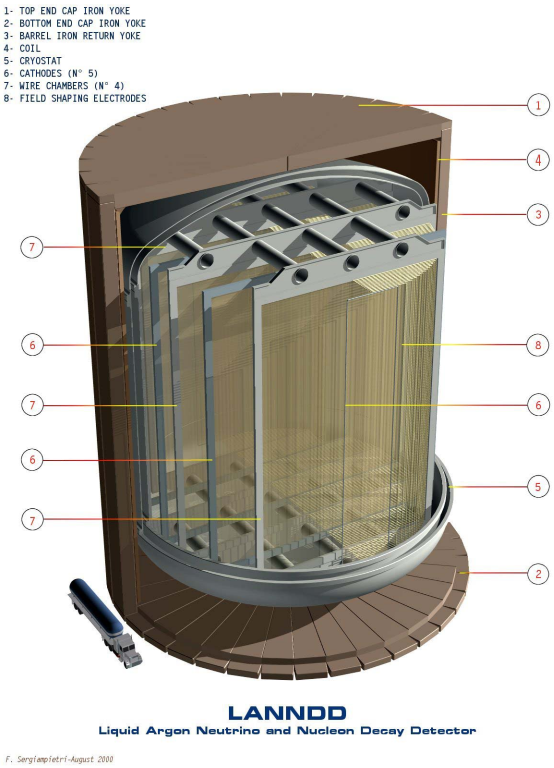

FIG. 5. Concept of a 70-kton Liquid Argon Neutrino and Nucleon Decay Detector (LANNDD) [42,43].

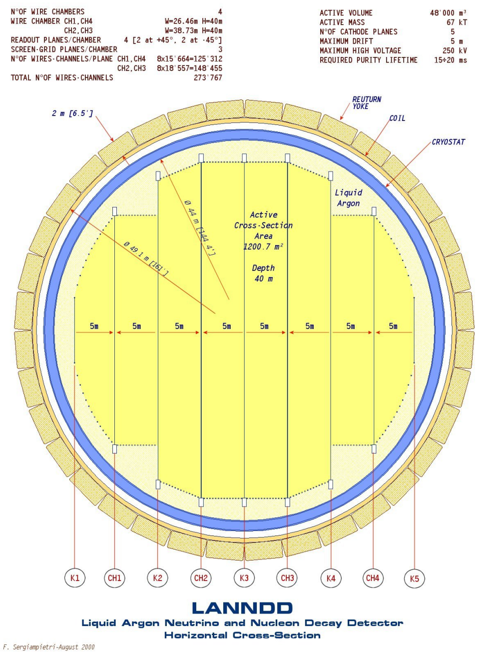

FIG. 6. Top view of the electrode arrangement of a 70-kton Liquid Argon Neutrino and Nucleon Decay Detector (LANNDD) [43].

The data acquisition for a liquid-argon TPC can operate in a pipelined, deadtimeless mode, with zero-suppression [44], technical aspects of which are illustrated in Figs. 7-9. This could permit fully live operation at the Earth's surface for nucleon decay studies, in addition to triggered data collection of neutrino interactions from a pulsed accelerator beam. The data rate would, of course, be quite high in this case. It may nonetheless be less costly to implement a high rate data-acquisition system than to reduce the untriggered data rate by siting the detector deep underground.

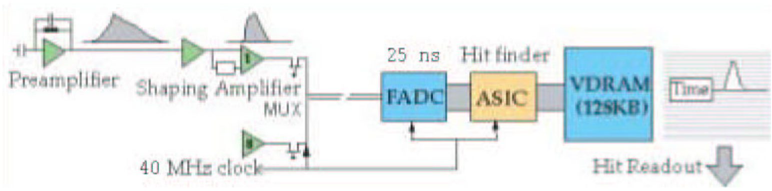

FIG. 7. Scheme of the front-end electronics of the ICARUS detector [44].

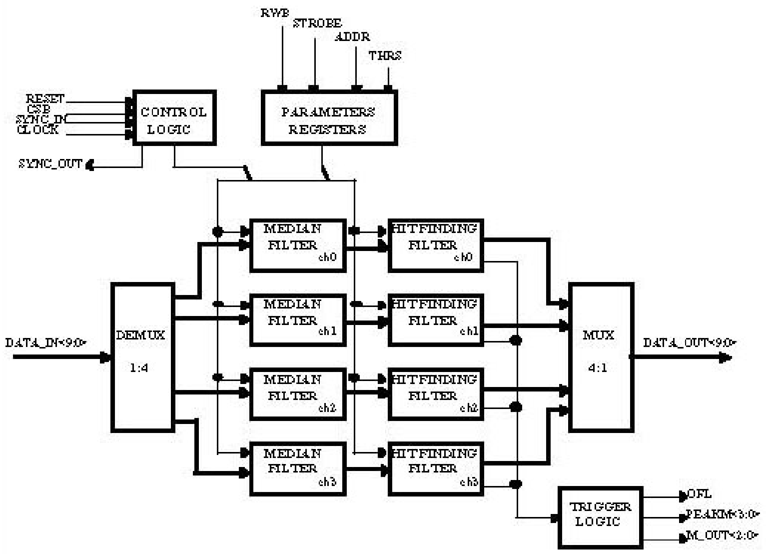

FIG. 8. Scheme of the back-end electronics of the ICARUS detector [44].

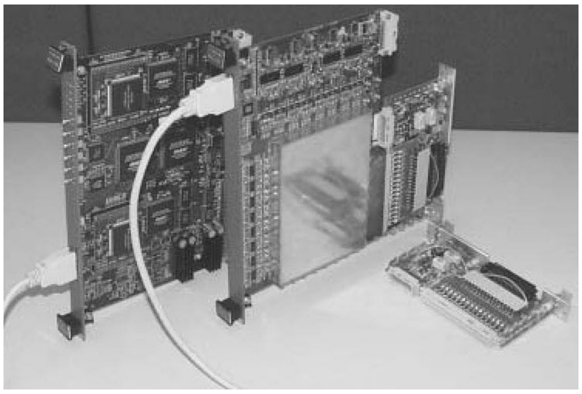

FIG. 9. Readout electronics modules of the ICARUS detector [44].

In the future, neutrino beams from pion decay may be supplanted by those from muon decay [45], in which cases beams of ν_μ and $\bar{\nu}_e$ or $\bar{\nu}_\mu$ and ν_e would be available. To take advantage of such beams for studies of CP violation, the sign of the final state lepton much be determined in the detector, which must therefore be immersed in a magnetic field. A liquid argon TPC is compatible with a superimposed magnetic field. The sign of muons of any energy could be well determined with a field of only 0.1 T, and the sign of electrons up to a few GeV energy could be determined in a field of 0.5 T by analysis of the curvature of tracks in the electromagnetic shower [46–48].

1. Fiducial Mass

If the liquid argon detector is constructed in the form of a right circular cylinder of radius r and height $h = 2r$, then the volume is $V = 2\pi r^3$, and the total mass of argon (density 1.4

metric tons/m^3) is

$$M_{\text{total}}(\text{tons}) = 2.8\pi r^3, \tag{5.1}$$

for radius r in meters.

Because the time projection chamber has electrodes at 250 kV, the instrumented volume must be set back from the cryostat wall by some distance ≈ 0.5 m. Therefore, the instrumented mass of argon is

$$M_{\text{instrumented}}(\text{tons}) = 2.8\pi(r - 0.5)^3 \approx \left(1 - \frac{1.5}{r}\right) M_{\text{total}}. \tag{5.2}$$

The fiducial volume is smaller than the instrumented volume because a neutrino interaction must be well contained within the detector to be useful in the physics analysis. Taking the physics emphasis to be electron neutrino appearance events, the characteristic volume of an interaction is a cylinder of about 3 radiation lengths radius (0.5 m) and about 18 radiations lengths deep (2.5 m). The events should not start closer than, say, 0.5 m from the edge of the instrumented volume, to insure that they originate from a neutral particle. Hence the radial depth of the fiducial volume is less than that of the instrumented volume by $(2.5 + 0.5)/2 = 1.5$ m, while the radial height and width are smaller by 0.5 m. These offsets must be combined with the high-voltage offset of 0.5 m, leading to the expression

$$M_{\text{fiducial}}(\text{tons}) = 2.8\pi(r - 2)(r - 1)^2 \approx \left(1 - \frac{4}{r}\right) M_{\text{total}}, \tag{5.3}$$

which is illustrated in Fig. 10.

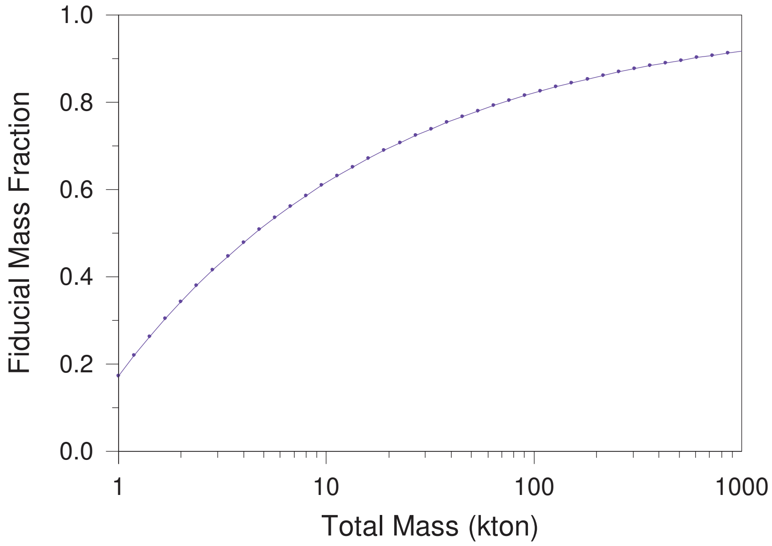

FIG. 10. The fraction of the total mass of liquid argon detector that is in the fiducial mass for detection of electron neutrino appearance events, according to expression (5.3).

2. Readout Channel Count

The instrumented volume of a liquid argon time projection chamber is organized into a set of cells of depth 3-5 m along the direction of the electric field (≈ 500 V/cm), as illustrated in Fig. 6 for a 70-kton detector.

In a typical gas-phase TPC, the ionization electrons drift to an anode-wire plane at which Townsend amplification occurs, and the readout is based on time digitization of the induced signal size on pads on a nearby cathode plane.

In a liquid argon TPC no amplification of the ionization electrons is required, as a minimum ionizing particle creates about 50,000 electron-ion pairs per cm. However, the use of a pad readout plane would lead to a prohibitively large channel count. Instead, the signals are detected on two (or three) crossed wire planes (per cell). The ionization electrons pass by the first (and second if a total of three) of these planes, inducing signals on the wires, and are then collected on the second (or third) plane. The use of three readout planes, x-u-v, allows superior rejection of "ghost" images in case of multiple "hits" within a given time slice.

For operation of a large detector at the Earth's surface, it may be preferable to have three readout planes to provide greater separation of neutrino events from "accidental" cosmic-ray events.

The ICARUS detector uses three readout planes, with a wire spacing of 3 mm on each plane. The time-sampling frequency of 2.5 MHz corresponds to sampling over 0.6 mm along the drift direction. Thus, the effective pixel size of the ICARUS readout is $3 \times 3 \times 0.6$ mm^3.

The maximum wire length in the present ICARUS detector is amount 9 m. It is proposed that longer wires be used in a larger detector, so that all wire connections can be made near the outer surface of the detector. Longer wires have larger capacitance (proportional to their length), and hence a given charge leads to a smaller voltage signal. As the present ICARUS detector operates near the limit of acceptable signal/noise, some change will have to be made for successful operation with longer wires.

A simple solution is to increase the wire spacing from 3 mm by the factor $L/9$, where L is the wire length. This increases the signal in the same ratio, while the capacitance increases by $L/(9\ln(L/9))$, and the signal/noise ratio actually improves by $\ln(L/9)$.

Of course, this solution increases the effective pixel size in the two transverse coordinates (but not along the drift coordinate where the time sampling frequency determines the pixel size). Additional study is required to determine whether such larger pixels would have a detrimental effect on the identification of electron neutrino interactions against the background of neutral current interactions.

For the present study, we assume that use of a larger wire spacing and an x-u-v readout is appropriate for a large detector. For the particular example of a 100 kton detector ($r = 22.5$ m), where the wire length would be about 45 m, we considered use of a 1-cm wire spacing. The wire capacitance increases by $5/\ln 5 = 3.1$ compared to 9-m-long wires, and the signal size is 3.3 times larger than that for 3-mm wire spacing. Then a cell arrangement similar to that shown in Fig. 6 (but with 10 cells of depth 4.4 m rather than 8 cells of 5-m depth) leads to a channel count slightly less than 300,000.

The channel count for detectors of other mass is scaled from this number according to the surface area, *i.e.*, as $M^{2/3}$.

3. Preliminary Cost Estimate

As well as being the highest-performance large detector for neutrinos, a liquid argon TPC is also one of the least costly. We have made a preliminary cost estimate for a 100 kton detector, assigning costs in two categories:

1. Costs proportional to detector mass.

   (a) Liquid argon @ \$700k/kton (delivered to a site in Minnesota) based on a preliminary budget estimate from the largest USA vendor of argon [49].

   The annual production of liquid argon in the USA is about 1Mton, so filling of a large liquid argon detector in a timely manner is a significant perturbation on the entire USA market. The largest argon production facilities are located in Chicago and the Gulf Coast. To fill a 100 kton detector in one calendar year would require a tank truck every 2 hours, 24 hours a day.

   (b) The on-site cryogenic system for purification and recondensation of liquid argon, sketched in Fig. 11, is estimated to cost \$10M [50].

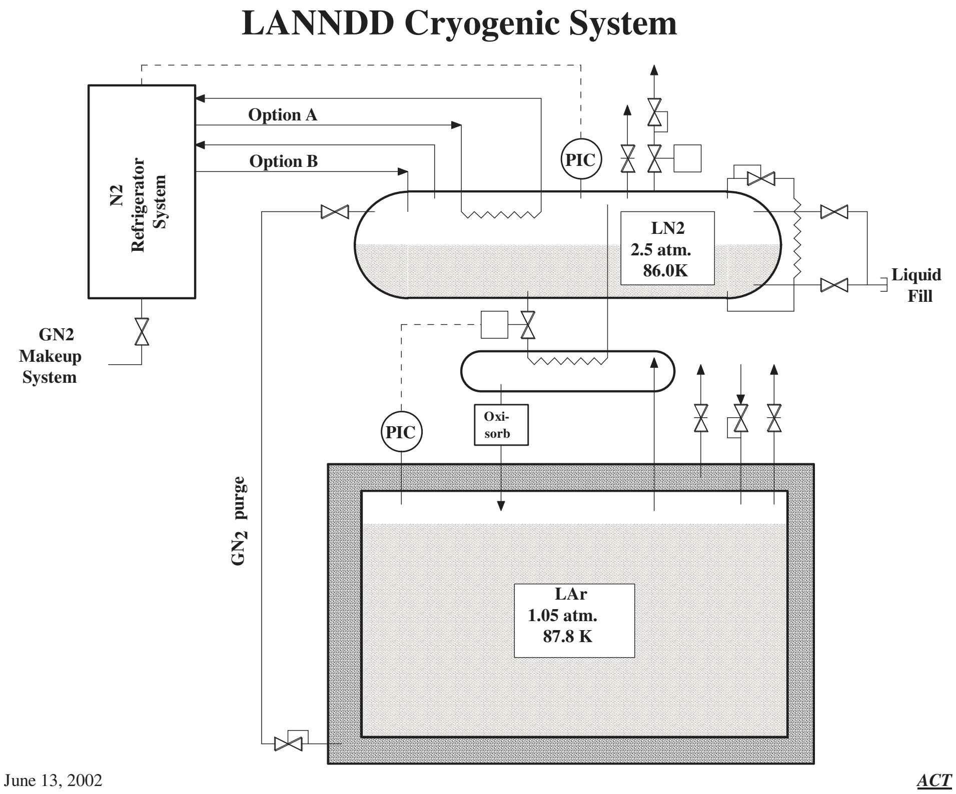

FIG. 11. Cryogenic system for a 100-kton liquid argon detector [50].

2. Costs proportional to detector surface area.

   (a) Site preparation, estimated at $10M.

   (b) Cryogenic storage tank, sketched in Fig.12, estimated at $20M based on a quotation from the leading USA vendor of liquefied natural gas storage tanks [50].

   The inner vessel of a large cryogenic storage tank is welded together from nickel-steel plates. Present welding technology limits the plate thickness to 60 mm, and consequently the present maximum height of a tank is 30-40 m. That is, tanks for more than 100 kton of liquid argon will require an advance in plate welding technology. Such advances are, of course, of interest to the tank manufacturers independent of our application.

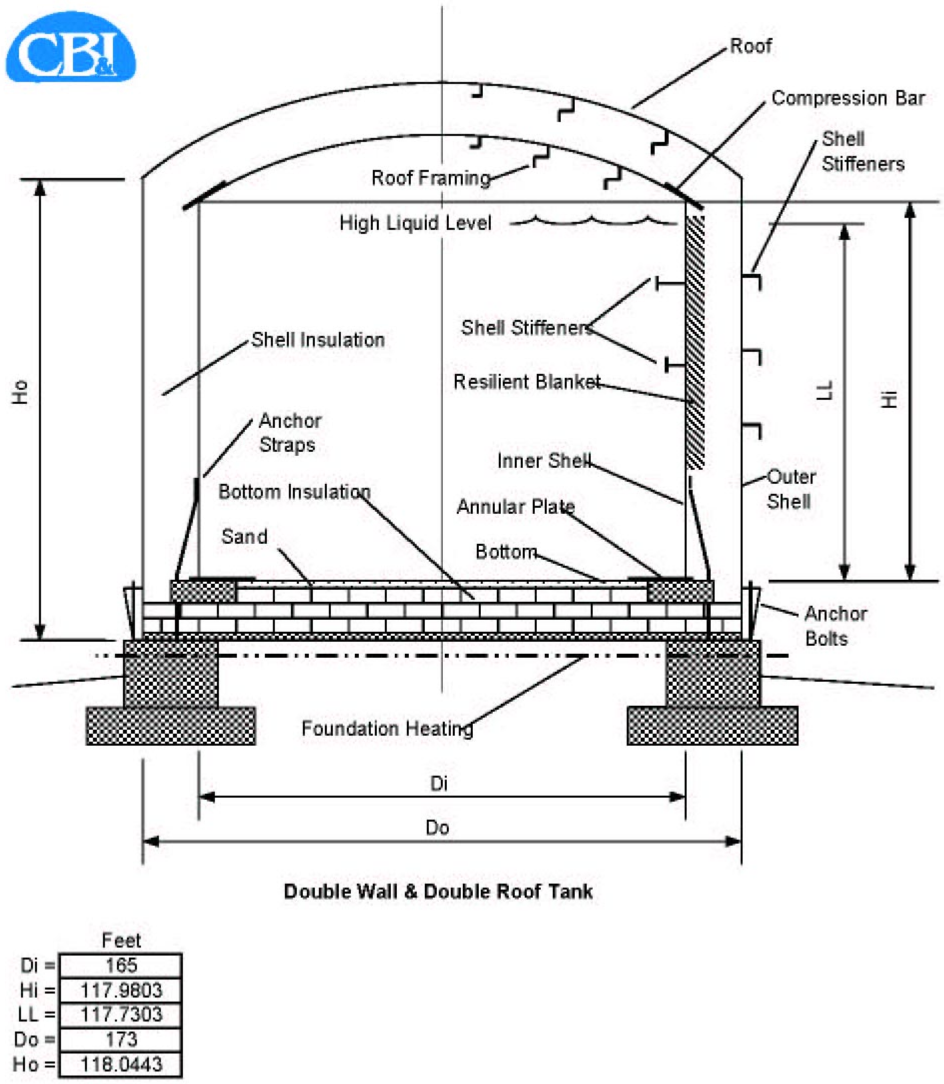

FIG. 12. Side view of the cryogenic storage tank for a 100 kton liquid argon detector, from a vendor quotation [50].

(c) Readout electronics, \$30M for 300k channels of commercial electronics designed for ICARUS, based on a discussion with CAEN [51].

If equivalent electronics were to be produced "in house" at Fermilab, the cost might be 30-50% less.

(d) Computer systems, estimated at \$10M.

In view of the very preliminary nature of these estimates, we add a 33% contingency. Table I summarizes this cost estimate.

TABLE I. Preliminary cost estimate for a liquid argon detector of 100 kton total mass.

Component	Cost
Liquid argon (industrial grade)	\$70M
Cryo plant, including Oxisorb purifiers	\$10M
Surface site preparation	\$10M
Cryogenic storage tank	\$20M
Electronics (300k channels)	\$30M
Computer systems	\$10M
Subtotal	\$150M
Contingency	\$50M
Total	\$200M

The cost estimate scales with total detector mass M in ktons according to

$$\text{Cost in \$M} = 1.333\left[80\frac{M}{100} + 70\left(\frac{M}{100}\right)^{2/3}\right]. \tag{5.4}$$

Figure 13 shows the results of this algorithm. The cost estimate as a function of fiducial mass can now be obtained using eq. (5.3), with results shown in Fig. 14.

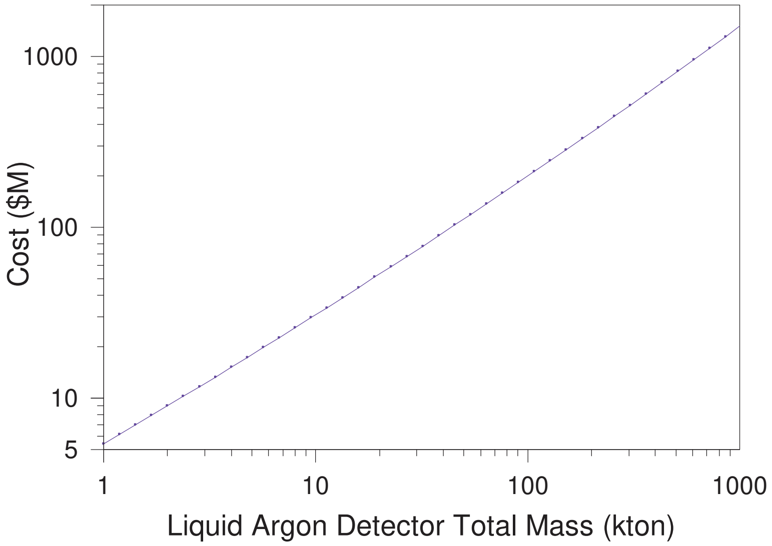

FIG. 13. Preliminary cost estimate of a liquid argon detector as a function of total mass, according to expression (5.4).

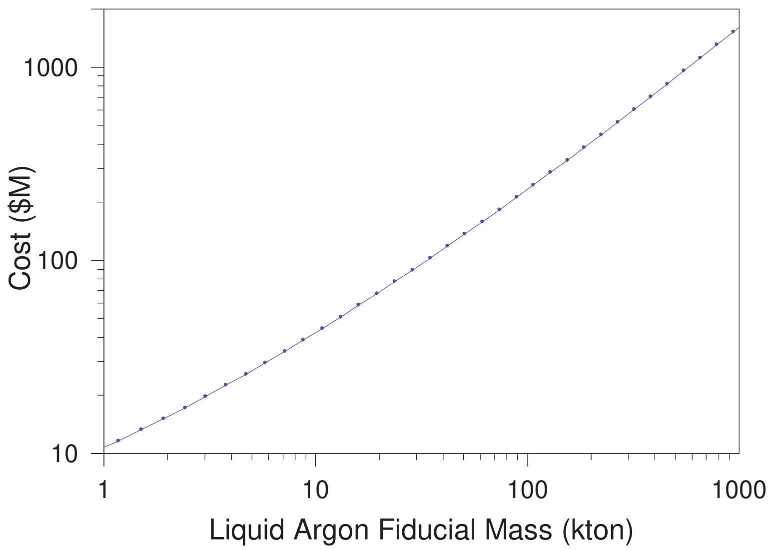

FIG. 14. Preliminary cost estimate of a liquid argon detector as a function of fiducial mass, according to expressions (5.3) and (5.4).

4. R&D Program

The ICARUS project continues to be the major source of R&D into hardware, software, and simulation of liquid argon time projection chambers. However, the ICARUS concept is presently limited to modules of about 1 kton. Before a larger module could be constructed, several issues should be addressed by additional R&D activity.

Hardware R&D Topics

1. Liquid-phase purification of industrial grade argon via Oxisorb.
2. Mechanics and electronics of wires up to 60-m long.
3. Cryogenic feedthroughs, possibly including buffer volume at 150K for low-noise FET's.
4. Verification of operation of a liquid argon TPC at 10 atmospheres (as at bottom of a 100-kton tank).
5. For eventual use at a neutrino factory, verification of operation of a liquid argon TPC in a magnetic field, including identification of the sign of electron charge.

R&D proposals to study items 4 and 5 have been submitted [47,48,52], but not yet funded. New initiatives are needed to address items 1-3, and the following:

Simulation Studies

1. What is maximum wire spacing consistent with good background rejection of neutral current events, *i.e.*, good π^0 identification?
2. What is shallowest depth at which a proton decay search can be performed to 10^{35} year for $p \to e^+\pi^0$ and $p \to K^+\bar{\nu}$?

C. R& D Issues for Liquid Argon Detectors

D. Water Cherenkov Detectors

(** Mark Messier)

E. R& D Issues for Water Cherenkov Detectors

F. Water Rich Detectors

(Scott Menary)

G. R& D Issues for RICH Detectors

H. KamLAND-like Detectors

I. R& D Issues for KamLAND-like Detectors

VI. SAMPLING DETECTORS

A. Absorber Issues

1. steel

(** Jeff Nelson)

2. plastic

(** Jeff Nelson)

3. water

(** Jeff Nelson)

4. cheap low Z material

Coal, walnuts, cracked corn...

B. Solid Scintillator Detectors

(Mayda Velasco)

C. Solid scintillator

Solid scintillator technology has a long and successful tradition in particle physics experiments, including several projects at FNAL. These traditions involve past and current local R&D and construction efforts, ranging from MINOS, through CDF and D0 to CMS, as well as designs of the neutrino oscillation project P860 and the STAR experiment. All those projects triggered a lot of R&D activity on the production of high quality a lower cost extruded scintillator at Fermilab. The detector element consists of a solid material with scintillating properties, a WLS fiber, a light guide and signal amplifier. A traversing charged particle loses energy in the scintillator, a part of it characterized by the quantity called scintillation efficiency, $\epsilon \sim 3\%$, is deposited in form of light. Part of this light, defined by the fiber capture efficiency $\chi \sim 5\%$, is transported through the light guide and amplified by a quantity Θ being a product of the Quantum Efficiency and the gain, the latter being typically of the order of $5{\times}10^4$. The Quantum Efficiency of typical photomultipliers, used e.g. in MINOS, is of the order of 13%.

Extensive physics studies have been done based on a fine grained steel-scintillator design and most of our present knowledge of the physics potential of NuMI Off-axis comes from simulations and Monte Carlo analysis involving this particluar design.

D. R&D issues for solid scintillator

A complete in-house facility at Fermilab includes a Scintillator Detector Development Laboratory, a Thin-Film facility, CNC routing and machine development. The production of extruded scintillator may today proceed at a rate four times higher than that for MINOS, better quality and some cost reduction over MINOS are also expected, the latter falling possibly below $5 per kg.

Other, perhaps more challenging, R&D issues involve the fiber and photodetector. Readout optimization is a major component that largely defines the overall cost of the detector. Given a 5 times higher longitudinal and 2 times higher transverse segmentation than that of the MINOS far detector, as well as a 4 times greater detector mass, a linear extrapolation of the corresponding MINOS costs would lead to unacceptably large numbers. Essential cost reduction can be obtained by applying currently available new technologies which have appeared since the time of the MINOS far detector design. Replacing the standard MINOS PMT readout by a VLPC based one results in an increase of the Quantum Efficiency from 13% to ~80-85%. This enables a reduction of the original MINOS fiber diameter of 1.2 mm to 0.4 mm while keeping a similar overall detector performance. Tests have been carried on which showed that an even better performance (in number of photoelectrons) can be currently achieved with a 0.5 mm fiber and VLPC readout compared to the original MINOS setup (1.2 mm fiber, PMT readout). [Show figure from A.Bross]. As both fiber and photodetector costs go like the cross-sectional area, this opens the possibility of an least ten-fold cost reduction. Although at present relevant data exist only for the MINOS 4 cm wide extrusions, it is expected that going to a 2 cm extrusion, as proposed for NuMI Off-axis, may only improve somewhat the results. Additional tests with different extrusions and the latest

VLPC type are due to become available shortly. On the other hand, 0.4 mm is believed to be near to the critical fiber diameter below which light transportation ceases and this marks the borderline of a possible cost reduction by going to thinner fiber.

The same data from the MINOS extrusion studies indicate a light attenuation length along the fiber of $\sim$5 meters for a single ended readout. Accordingly, double sided readout was chosen for MINOS to ensure a secure light yield at all positions. The price is a two-fold increase in the number of readout channels. In a larger detector (a detector 12 meters across is considered in the steel-scintillator design), the issue is yet more important. It has been proposed to overcome this problem by applying the technique of mirroring of the far end light. Tests of the D0 fiber tracker indicate that an effective attenuation length of as much as 16 meters is obtained with a single ended readout and far end mirroring. This renders a single ended readout completely sufficient for a 12 meters large detector. With all the above modifications, the obtained light yield can be expected to be equal to or larger than that of the MINOS detector at any position.

A ten-fold cost reduction of the fiber is followed by a similar cost reduction of the photodetector. A 5×10 element array with a 0.4 mm fiber would cost the same or less than a 2×4 element array with a 1 mm fiber used at D0 (about \$240). Although a 10 times higher density requires cold end electronics, this technology has been successfuly applied in the past by Boeing. R&D work on the next generation VLPC's is currently under way in the Lawrence Semiconductor Research Laboratory (LSRL), which has collaborated with Boeing, has been previously awarded a phase I R&D grant and recently a new phase II grant for this purpose. Their research aims at producing high density VLPC arrays and demonstrating an order of magnitude cost reduction compared to D0.

From all the presently known input, the total cost of a 20 kton steel-scintillator detector has been recently estimated to about \$100 M. The ongoing extensive R&D activity in the field can be expected to further reduce this number in the following years.

E. R& D Issues for Solid Scintillator Detectors

F. Liquid Scintillator Detectors

(Ken Heller)

G. R& D Issues for Liquid Scintillator Detectors

H. RPC/gas Detectors

(Peter Shanahan)

I. R& D Issues for RPC/gas Detectors

J. Emulsion Detectors

K. R& D Issues for Emulsion Detectors

VII. OTHER R& D ISSUES

A. cross sections

(** Kevin McFarland)

B. pion yields

(**Mark Messier)

C. targetry

(** Mikhail Kostin, Nikolai Mokhov)
(** Mikhail Kostin, Nikolai Mokhov)
The target will remain the most critical device in the NuMI beamline after upgrade of the Fermilab accelerator complex with a Proton Driver. The target must be able to survive a 2MW proton beam with some safety margin. A good target for a neutrino superbeam facility would satisfy the following conditions: it survives one spill; a steady state temperature must not exceed a temperature stress limit; the target life time is greater than 6 months; in the case of multiple choice for a target candidate, the optimal target is the one that provides the highest π^+ yield in the energy interval of interest. The first three clauses are quite obvious. The last one is driven by the physics case. An off-axis neutrino beam of a required energy of ≈ 3 GeV will be formed by secondary pions with energy in the 6–14 GeV interval. Not all the pions of such energy will contribute to neutrino beam. A beamline focusing system acts differently on pions with different transverse momentum. Moreover, the focusing system itself would not be necessarily same for different targets. Therefore we use a simplified approach for these studies. An integrated over p_T pion flux is used for the target optimization.

1. What survives one spill ?

A number of commonly used materials was considered for a target. The target was simulated with the MARS14 code [30]. We assumed that a 120 GeV proton beam hits a rod target with a length of two interaction lengths. For the first trial, the beam was assumed to be a Gaussian with $\sigma_x = \sigma_y = 1$ mm (approximately NuMI parameters). The target radius R_T was optimized for the maximal pion yield scanning the radius of target with a step of 0.5 mm starting from 2.5 mm (see Table II). In order to achieve a power of 2 MW, the nominal NuMI beam intensity is rescaled by a factor of 5 that corresponds to 2×10^{14} protons per spill. We also assumed that the Main Injector repetition period of 1.9 s does not change.

Calculated peak energy deposition densities (ED) on a beam axis are shown in Table II for C through Hg targets. For the beam conditions described above all the materials experience a significant thermal shock. The stress limits known for graphite, nickel and inconel are about 1000 J/g. The limit for copper is about 600 J/g. As one can see from the table, none of the solid materials can survive such conditions.

Despite the fact that the above conditions are not operable for the solid materials, it is interesting to notice that the pion yield in the defined energy interval does not vary significantly with the target material (Table II). Fig. 15 shows the pion yield versus pion energy for graphite and mercury. Much more soft pions are produced in a mercury target. But what is important, the yield is about the same in the energy region of interest. Pion spectra for the other materials studied behave similarly.

The most obvious idea of stress reduction is to increase the beam transverse spot size. In the study below, both the beam spot size $\sigma = \sigma_x = \sigma_y$ and target radius R_T are varied. For a graphite target the pion yield as a function of R_T/σ is shown in Fig. 16 for different σ. As one can see the variation of the maximal yeild for different σ does not exceed 7%. This is due to the fact that pions leave the target at much larger angle than a specific angle at which the target collimates the pions, that is $\mathrm{atan}(\mathrm{R}_T/\lambda_I) \approx 1^\circ$ (Fig. 17). Energy deposition in the hottest cell of target is acceptable at $\sigma > 1.5$ mm (Fig. 18). For example, for σ=3 mm and target radius R_T=9 mm the peak energy deposition is 310 J/g that is well below the limit. Thus the beam spot size and target radius for graphite can be substantially increased compared to the NuMI parameters without significant loss of the yield.

Material	Peak ED (J/g)	π^+yield (N/POT)	optimal R_T (mm)
Graphite	1581 ± 18	0.754 ± 0.007	5.0
Nickel	6520 ± 251	0.684 ± 0.006	2.5
Inconel	6011 ± 259	0.699 ± 0.006	3.0
Copper	6084 ± 216	0.690 ± 0.006	2.5
Indium	5248 ± 149	0.752 ± 0.006	3.0
Mercury	10064 ± 293	0.715 ± 0.006	3.0

TABLE II. Density of peak energy deposition and pion yield in the 6–14 GeV interval for various targets. Also shown are the optimal target radii R_T for σ=1 mm.

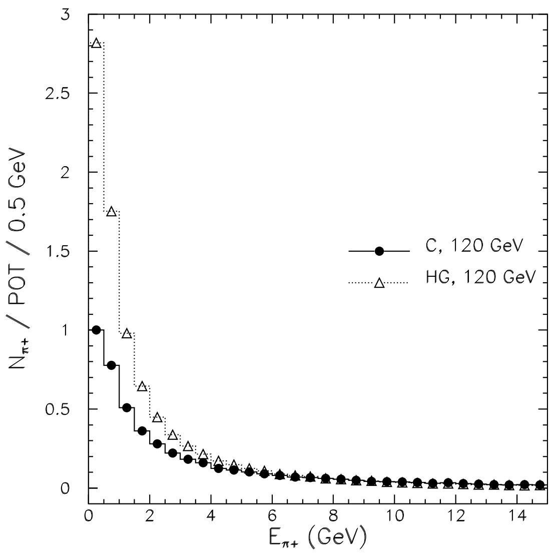

FIG. 15. Pion yield versus pion energy. The distributions are normalized per the number of protons on target (POT).

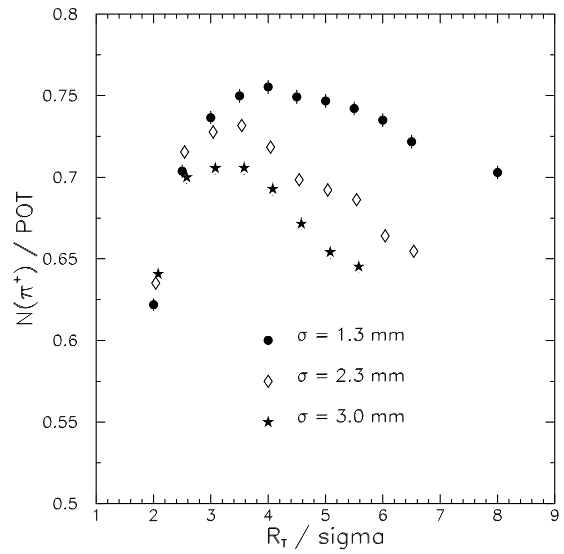

FIG. 16. Number of π^+ coming from a graphite target in the interval 6–14 GeV against the value of target radius over beam sigma. Shown are dependencies for different beam RMSs.

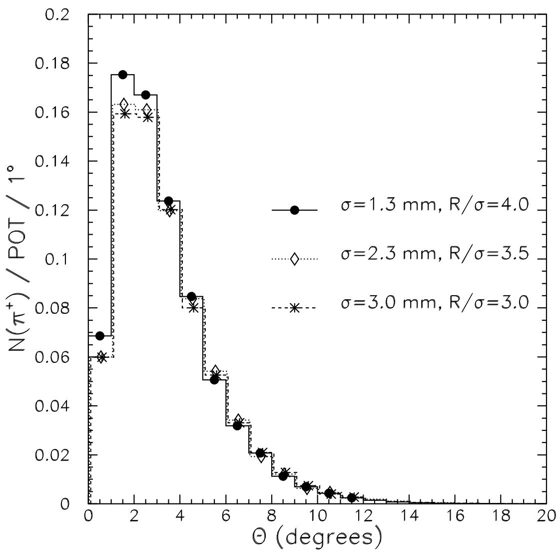

FIG. 17. Angular distributions for pions coming off a graphite target. θ is an angle between the target axis and pion direction.

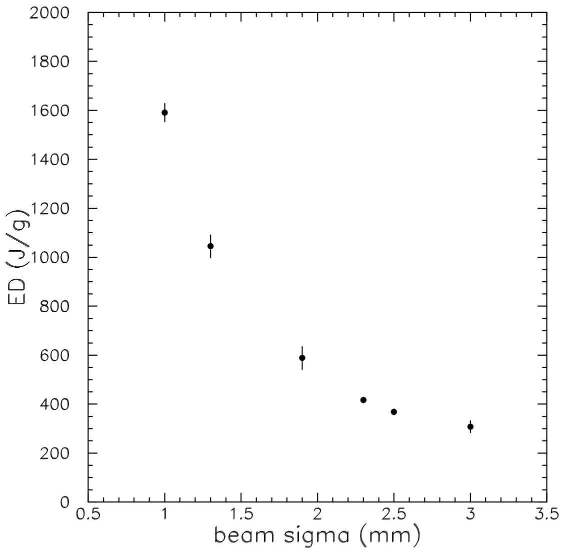

FIG. 18. Energy deposition in the hottest cell of a graphite target versus beam spot size.

The same idea does not work well for solid dense materials. An attempt to bring the energy deposition safely below the limit by increasing σ and R_T results in a substantial reduction of the pion yield. For example, if one increases the beam σ up to 12.5 mm keeping the ratio to be optimal $R_T/\sigma = 2.5$, the pion yield from an inconel target reduces down to 0.43 pions per proton that is much smaller than the yield of about 0.71 from an optimal graphite target. The density of peak energy deposition is 1250 J/g in this case that is still above the limit.

The studies performed show that graphite is the most convenient material for a FNAL neutrino superbeam facility. Indeed, the dense solid materials do not provide enough of pion flux at the acceptable beam and target radii. The use of light materials with large interaction lengths such as Li and Na will lead to a too long target, making focusing of secondaries problematic. A mercury jet target seems to be too complex, expensive and hazardous device and at the same time it does not provide any advantages over a graphite target for the given experimental conditions.

2. Target life-time

One of the factors limiting the target life-time is radiation damage. The life-time determined here corresponds to the time when 5 dpa (displacements per atom) occur in the hottest cell of the target. The atoms are displaced due to interactions with hadrons with kinetic energy of >0.1 MeV. The 5 dpa limit corresponds to the integrated hadron flux of about 5×10^{22} cm^{-2}. From the MARS simulations we have found that for the beam σ=3mm and graphite target radius R_T=9mm the limit of 5 dpa is reached within 5 years and 8 months assuming 10 months of operation per year at the full intensity.

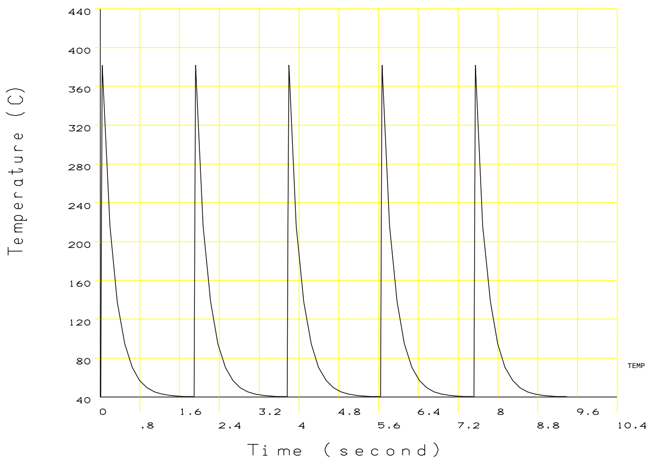

FIG. 19. Temperature evolution in the hottest cell of a graphite target with 1.9 s repetition rate.

3. Temperature buildup

The temperature evolution in a graphite target has been investigated with the ANSYS code [53]. An ED distribution in a target with R_T=9mm was simulated with MARS. The beam σ was chosen to be 3mm. The temperature rise for the target elements was estimated from the ED distribution and was assumed to be instant. The temperature rise was applied to the target every 1.9 sec. A simplified cooling system was used in this simulation. The heat excess was brought away from the target by water with constant temperature of 40° C running around the outer cylindrical surface of the target. As Fig. 19 shows, the temperature in the hottest cell oscillates between 40° C and 380° C without any buildup. The tensile stress obtained from the simulation is about 20 MPa at the tensile strength for graphite of about 90 MPa.

4. Conclusions

A graphite target represents a simple and cheap solution for the FNAL neutrino superbeam facility. Such a target satisfies all the requirements applied: it survives one spill; radiation damage does not constrain the life-time significantly; there is no temperature buildup in target; pion yield is quite high.

D. Proton Intensity

Doug Michael?

VIII. SUMMARY AND CONCLUSIONS

[1] Recent solar data is in S. Fukuda, et al. Phys. Rev. Lett. **86**, 5651 (2001), S. Fukuda et al., *ibid*, 5656 (2001) (SuperKamiokande) and Q.R. Ahmad et al., Phys. Rev. Lett. **87**, 071301 (2001), nucl-ex/0204008, nucl-ex/0204009 (SNO). The Homestake, Kamiokande, GALLEX, and SAGE experiments provided earlier data.

[2] See, for example, Q.R. Ahmad et al. in [1].

[3] Y. Fukuda et al., Phys. Lett. **B433**, 9 (1998); Phys. Rev. Lett. **81**,1562 (1998); *ibid.*, **82**, 2644 (1999); Phys. Lett. **B467**, 185 (1999) (SuperK). Other data is from the Kamiokande, IMB, Soudan-2, and MACRO experiments; see, e.g., talks at Neutrino-2000, Neutrino-2002.

[4] S. H. Ahn et al., Phys. Lett. **B511**, 178 (2001); J. Hill, talk at the NOON Conf. (Dec., 2001).

[5] M. Apollonio et al., Phys. Lett. **B420**, 397 (1998); Phys. Lett. **B466**, 415 (1999).

[6] C. Athanassopoulous et al., Phys. Rev. Lett. **77**, 3082 (1996); Phys. Rev. Lett. **81**, 1774 (1998); A. Aguilar et al., hep-ex/0104049.

[7] M. Steidl for the KARMEN Collaboration, Nucl. Phys. Proc. Suppl. **100**, 188 (2001).

[8] See http://www-numi.fnal.gov/ .

[9] See http://www-boone.fnal.gov/ .

[10] See http://proj-cngs.web.cern.ch/proj-cngs/.

[11] See http://neutrino.kek.jp/jhfnu, in particular, Y. Itoh et al., "Letter of Intent: A Long Baseline Neutrino Oscillation Experiment using the JHF 50 GeV Proton Synchrotron and the Super-Kamiokande Detector" (Feb. 2000); Y. Itoh et al, "The JHF-Kamioka Neutrino Project", hep-ex/0106019.

[12] V. Barger et al. (Fermilab Superbeam Working Group), Nov., 2000, hep-ph/0103052.

[13] V. Barger, S. Geer, R. Raja, and K. Whisnant, Phys. Rev. **D63**, 113011 (2001).

[14] I. Mocioiu and R. Shrock, JHEP 0111, 050 (28 pages) (2001).

[15] UNO Protocollaboration and Theoretical Advisory Committee, 'Physics Potential and Feasibility of UNO", UNO Snowmass 2001 White Paper, June, 2001.

[16] Snowmass E1 Working Group (T. Adams et al.), E1 Working Group Summary: Neutrino Factories and Muon Colliders, hep-ph/0111030.

[17] W. Chou, ed. "Proton Driver Design Study", Fermilab-TM-2136 (2001).

[18] G. Barenboim et al., hep-ph/0204208.

[19] G. Barenboim, A. de Gouvea, T. Dombeck, N. Grossman, D. Harris, D. Michael, M. Szleper, M. Velasco, and S. Werkema, hep-ex/0206025.

[20] C. Albright et al. (Fermilab Neutrino Factory Physics Working Group), "Physics at a Neutrino Factory", Apr. 2000, hep-ph/hep-ex/0008064. (See also the companion machine study "Feasibility Study of a Neutrino Factory Based on a Muon Storage Ring", by the Fermilab Neutrino Factory Feasibility Study Working Group, N. Holtkamp, et al.)

[21] Muon Collider and Neutrino Factory Collaboration, "Neutrino Factory Feasibility Study II" (May 2001), available at http://www.cap.bnl.gov/mumu.

[22] e.g., K. McDonald and R. Shrock, talks at Snowmass 2001, June, 2001; W. Marciano, hep-ph/0108181; A. Mann et al. (3M Protocollaboration), "Megaton Modular Multi-Purpose Neutrino Detector" (Nov. 2001); D. Beavis et al., Neutrino Oscillation Experiments for Precise Measurements of Oscillation Parameters and Search for Muon-Neutrino to Electron Neutrino Appearance and CP Violation: Letter of Intent to Brookhaven National Laboratory", hep-ex/0205040.

[23] L. Wolfenstein, Phys. Rev. **D17**, 2369 (1978); S. P. Mikheyev and A. Smirnov, Yad. Fiz. **42**, 1441 (1985) [Sov.J. Nucl. Phys. **42**, 913 (1986)], Nuovo Cim., **C9**, 17 (1986).

[24] V. Barger, K. Whisnant, S. Pakvasa, and R. J. N. Phillips, Phys. Rev. **D22**, 2718 (1980); P. Krastev, Nuovo Cimento **103A**, 361 (1990); R. H. Bernstein and S. J. Parke, Phys. Rev. **D44**, 2069 (1991); De Rujula, M. B. Gavela, and P. Hernandez, Nucl. Phys. **B547**, 21 (1999); P. Lipari, Phys.Rev. **D61**, 113004 (2000) S. Dutta, R. Gandhi, and B. Mukhopadhyaya, Eur.Phys.J. **C18**, 405 (2000); V. Barger, S. Geer, K. Whisnant, Phys.Rev. **D61**, 053004 (2000); D. Dooling, C. Giunti, K. Kang, C. W. Kim,Phys.Rev. **D61**,073011 (2000); A. Bueno, M. Campanelli, A. Rubbia, Nucl.Phys. **B573**, 27 (2000); V. Barger, S. Geer, R. Raja, K. Whisnant, Phys.Rev. **D62**, 013004 (2000); M. Freund, M. Linder, S.T. Petcov, A. Romanino, Nucl.Phys. **B578**, 27 (2000); I. Mocioiu and R. Shrock, AIP Conf.Proc. **533**, 74 (2000) (NNN99); I. Mocioiu and R. Shrock, Phys.Rev. **D62**, 053017 (2000); V. Barger, S. Geer, R. Raja, K. Whisnant, Phys.Rev. **D62**, 073002 (2000); A. Cervera, A. Donini, M.B. Gavela, J. Gomez Cadenas, P. Hernandez, O. Mena, and S. Rigolin, Nucl.Phys. **B579**, 17 (2000), Erratum-ibid. **B593**, 731 (2001); M. Freund, P. Huber, M. Lindner, Nucl.Phys. **B585**, 105 (2000); V. Barger, S. Geer, R. Raja, K. Whisnant, Phys.Lett. **B485**, 379 (2000); Z.-Z. Xing, Phys. Lett. **487**, 327 (2000); Phys. Rev.

D63, 073012 (2000); A. Bueno, M. Campanelli, A. Rubbia, Nucl.Phys. **B589**, 577 (2000); P. Fishbane, Phys. Rev. **D62**, 093009 (2000); P. Fishbane and P. Kaus, Phys. Lett. **B506**, 275 (2001); P. Fishbane and S. Gasiorowicz, hep-ph/0012230; V. Barger, S. Geer, R. Raja, K. Whisnant, Phys.Rev. **D63**, 033002 (2001); M. Freund, P. Huber, M. Lindner, hep-ph/0105071. E. Akhmedov, A. Dighe, P. Lipari, A. Smirnov, Nucl. Phys. **B542**, 3 (1999); E. Akhmedov, Nucl.Phys. **B538**, 25 (1999); E. Akhmedov, hep-ph/0001264; E. Akhmedov, P. Huber, M. Lindner, and T. Ohlsson, hep-ph/0105029; J. Arafune, J. Sato, Phys.Rev. **D55**, 1653 (1997); H. Minakata, H. Nunokawa, Phys.Rev. **D57**, 4403 (1998); M. Koike, J. Sato, hep-ph/9707203, Phys.Rev. **D62**, 073006 (2000).

[25] A. Romanino, Nucl.Phys. **B574** 675 (2000); S.M. Bilenky, C. Giunti, W.Grimus, Phys.Rev. **D58**, 033001 (1998); K. Dick, M. Freund, M. Lindner, A. Romanino, Nucl. Phys. **B562**, 29 (1999); M. Tanimoto, Phys. Lett. **B462**, 115 (1999); A. Donini, M.B. Gavela, P. Hernandez, S. Rigolin, Nucl.Phys. **B574**, 23 (2000); M. Koike, J. Sato, Phys.Rev. **D61**, 073012 (2000), Erratum-ibid. **D62**, 079903 (2000); S. J. Parke, T. J. Weiler, Phys.Lett. **B501**, 106 (2001); T. Miura, E. Takasugi, Y. Kuno, and M. Yoshimura, Phys. Rev. **D64**, 013002 (2001); M. Koike, T. Ota, J. Sato, hep-ph/0011387; P. Lipari. hep-ph/0102046.

[26] C. Jarlskog, Z. Phys. **C29**, 491 (1985); Phys. Rev. **D35**, 1685) (1987).

[27] V. Barger, S. Pakvasa, T. Weiler, and K. Whisnant, Phys. Rev. Lett. **85**, 5055 (2000); H. Murayama and T. Yanagida, Phys. Lett. **B520**, 263 (2001); G. Barenboim, L. Borissov, J. Lykken and A. Smirnov, hep-ph/0108199; G. Barenboim, L. Borissov, and J. Lykken, Phys. Lett. **B534**, 106 (2002); G. Barenboim, J. Beacom, L. Borissov, and B. Kayser, Phys. Lett. **B537**, 227 (2002); I. Mocioiu and M. Pospelov, Phys. Lett. **B534**, 114 (2002); A. Strumia, hep-ph/0201134.

[28] e.g., V. Barger, D. Marfatia, and K. Whisnant, hep-ph/0206038.

[29] D. Ayres et al. (A. Para, contact person), "Letter of Intent to Build an Off-Axis Detector to Study $\nu_\mu \to \nu_e$ Oscillations with the NUMI Neutrino Beam", June, 2002.

[30] N. V. Mokhov, "The MARS Monte Carlo", Fermilab FN-628 (1995); N. V. Mokhov and O. E. Krivosheev, "MARS Code Status", Fermilab-Conf-00/181 (2000); http://www-ap.fnal.gov/MARS/.

[31] "ANSYS (rev.5.1)", Swanson Analysis System, Inc., SASI/DN-P511:51, Houston (1994).

[32] C. Rubbia, *The Liquid Argon Time Projection Chamber: a New Concept for Neutrino Detector*, CERN-EP/77-08 (1977).

[33] D. Harris, *Comparison of Different Detectors with Same Beam*, presented at NNN02 (CERN, Jan. 18, 2002),
http://muonstoragerings.cern.ch/NuWorkshop02/presentations/harris.pdf

[34] ICARUS home page: http://www.aquila.infn.it/icarus/

[35] A. Rubbia, *Liquid Argon TPC and R&D*, presented at NNN02 (CERN, Jan. 17, 2002),
http://pcnometh4.cern.ch/pubs/nnn02.pdf

[36] The ICARUS Collaboration, *Cloning of T600 Modules to Reach the Design Sensitive Mass*, ICARUS-TM/01-09,
http://pcnometh4.cern.ch/Proposals/t2400doc_lowres.pdf

[37] A. Bueno, J. Rico and A. Rubbia *Spatial and Calorimetric Reconstruction of the ICARUS T600 Data*, ICARUS-TM/02-03 (May 21, 2002),

http://www.aquila.infn.it/icarus/icarus_tm/icarus_02_03.pdf

[38] The ICARUS Collaboration, *The ICARUS Experiment: a second-generation Proton decay experiment and Neutrino Observatory at Gran Sasso Observatory – Initial Physics Program*, ICARUS-TM/01-03 (Mar. 1, 2001),
http://www.aquila.infn.it/icarus/icarus_tm/icarus_01_03.pdf
A. Bueno *et al.*, *Nucleon decay searches: study of nuclear effects and background*, ICARUS-TM/01-04 (Oct. 9, 2001),
http://www.aquila.infn.it/icarus/icarus_tm/icarus_01_04.pdf

[39] Among a vast literature, see, for example, J.C. Pati, *With Grand Unification Signals in, Can Proton Decay be Far Behind?* (June 7, 2001), hep-ph/0106082.

[40] A. Bettini *et al.*, *A study of the factors affecting the electron lifetime in ultra-pure liquid argon*, Nucl. Instr. and Meth. **A305**, 177 (1991).

[41] In the USA, Oxisorb cartridges can be ordered from Frank Tamandl of MG Industries, Alllentown, PA, 610-530-5342,
http://www.mgindustries.com/gts/SpecGasEquip/Filtration.pdf

[42] D.B. Cline, F. Sergiampietri, J.G. Learned, K.T. McDonald, *LANNDD, A Massive Liquid Argon Detector for Proton Decay, Supernova and Solar Neutrino Studies, and a Neutrino Factory Detector* (May 24, 2001), astro-ph/0105442

[43] F. Sergiampietri, *On the Possibility to Extrapolate Liquid Argon Technology to a Supermassive Detector for a Future Neutrino Factory*, presented at NuFACT'01 (May 26, 2001),
http://www.hep.princeton.edu/~mcdonald/nufact/sergiampietri_nufact01.pdf

[44] See sec. 6.8 of [36].

[45] S. Ozaki *et al.*, eds., *Feasibility Study-II of a Muon-Based Neutrino Source* (June 14, 2001),
http://www.cap.bnl.gov/mumu/studyii/FS2-report.html

[46] A. Bueno, M. Campanelli and A. Rubbia, *Neutrino factories: Detector concepts*, presented at the IX Intl. Workshop on Neutrino Telescopes (Venice, Mar. 6-10, 2001),
http://pcicarus7.ethz.ch/Talks_pdfs/venice2001.pdf

[47] A. Badertscher *et al.*, *Magnetized Liquid Argon Detector for Electron Charge Sign Discrimination*, Letter of Intent to the CERN SPSSC (Jan. 3, 2002),
http://www.hep.princeton.edu/~mcdonald/nufact/uL@CERN_LOI.pdf

[48] M.V. Diwan *et al.*, *Proposal to Measure the Efficiency of Electron Charge Sign Determination up to 10 GeV in a Magnetized Liquid Argon Detector (μLANNDD)*, submitted to BNL (April 12, 2002),
http://www.hep.princeton.edu/~mcdonald/nufact/bnl_loi/argonprop.pdf

[49] Kate Loritz, Praxair Account Manager, *USA Liquid Argon Market Overview* (June 24, 2002),
http://www.hep.princeton.edu/~mcdonald/nufact/mulholland/Praxair_quotation.pdf

[50] G. Mulholland, *ELAN Detector Vessel Preliminary Study*, (May 17, 2002),
http://www.hep.princeton.edu/~mcdonald/nufact/mulholland/ELAN_Proposal.pdf

[51] Fabrizio Catarsi, CAEN Marketing Director, f.catarsi@caen.it, Bert Yost, bert.yost@caen,it.

[52] C. Lu and K.T. McDonald, *Studies of a Liquid Argon Time Projection Chamber in a Magnetic Field*, submitted to the DOE Advanced Detector Research Program (Oct. 30, 2001),
http://www.hep.princeton.edu/~mcdonald/nufact/argonprop_103001.pdf
bibitemMARS N. V. Mokhov, "The MARS Monte Carlo", Fermilab FN-628 (1995); N.

V. Mokhov and O. E. Krivosheev, "MARS Code Status", Fermilab-Conf-00/181 (2000); http://www-ap.fnal.gov/MARS/.

[53] "ANSYS (rev.5.1)", Swanson Analysis System, Inc., SASI/DN-P511:51, Houston (1994).